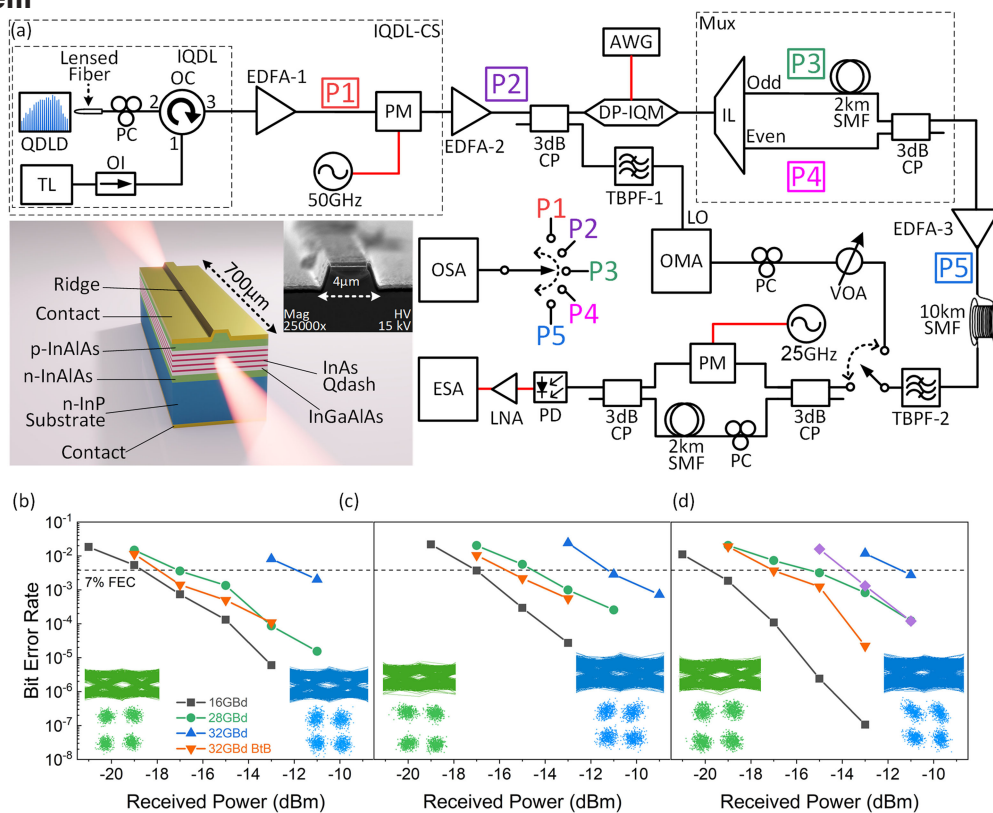# Injection-Locked Quantum-Dash Laser in Far L-Band 192 Gbit/s DWDM Transmission

Mohammed Zahed Mustafa Khan
Emad A. Alkhazraji
Amr Mohamed Ragheb
Maged Abdullah Esmail
Qazi Tareq
Habib Ali Fathallah
Khurram Karim Qureshi
Saleh Alshebeili

Injection-Locked Quantum-Dash Laser in Far L-Band 192 Gbit/s DWDM Transmission

Mohammed Zahed Mustafa Khan [1], **Emad A. Alkhazraji** [1,2]
Amr Mohamed Ragheb [3], **Maged Abdullah Esmail** [4], **Qazi Tareq,** [1]
Habib Ali Fathallah [5], **Khurram Karim Qureshi** [6]
and Saleh Alshebeili [3,7]

[1] Optoelectronics Research Laboratory, Electrical Engineering Department, King Fahd University of Petroleum and Minerals (KFUPM), Dhahran 31261, Saudi Arabia
[2] Department of Electrical and Electronic Engineering Technology, Jubail Industrial College, Jubail 31961, Saudi Arabia
[3] KACST-TIC in Radio Frequency and Photonics for the e-Society (RFTONICS), King Saud University (KSU), Riyadh 11421, Saudi Arabia
[4] Communications and Networks Engineering Department, Prince Sultan University, Riyadh 11586, Saudi Arabia
[5] Computer Department, Faculty of Sciences of Bizerte, University of Carthage, Tunis 1054, Tunisia
[6] Electrical Engineering Department, King Fahd University of Petroleum and Minerals (KFUPM), Dhahran 31261, Saudi Arabia
[7] Electrical Engineering Department, King Saud University (KSU), Riyadh 11421, Saudi Arabia

Abstract: Injection locked quantum-dash laser diode-based comb source is employed in wavelength-division multiplexed (WDM) optical transmission covering $\sim$1610 nm L-band optical telecommunication window. An aggregate data rate of 192 Gbits/s (3×32 GBaud-QPSK reaching 7% FEC overhead) is demonstrated over three 50 GHz separated channels in coherent transmission over a 10 km-long single mode fiber. A thorough investigation of the radio-frequency (RF) characteristics of all channels is carried out in terms of the linewidth, phase, and frequency noises, showing minimum values of 44 kHz, -80 dBc/Hz, and 5.2×10^{11} Hz^2/Hz, respectively. Also, an integrated average relative intensity noise of ~-132 dB/Hz is reported for the central channel. To the best of our knowledge, this constitutes the first report and demonstration of a dense WDM (DWDM) in an extended L-band regime using a comb source.

Index Terms: Quantum-dash, WDM transmission, L-band communication.

1. Introduction

The demands for ultrahigh bandwidth optical communication networks have been ever-intensifying owing to the sharp increase in both the number of end-users and their demand for high-speed mobile and internet connectivity. It is estimated that nearly one-third of the global population will have internet access by 2023 with 5.3 billion total internet users, while the annual internet traffic would reach 2.3 Zettabytes by the end of 2021 [1], [2]. In this respect, wavelength division multiplexed (WDM) based passive optical networks (WDM-PONs) show great promise by exploiting the huge bandwidth of optical fibers and providing simultaneous logical connectivity to multiple remote locations over a single physical point-to-multipoint fiber topology. WDM-PONs have been acknowledged as the ultimate solution for 10G, 100G, and 400G next generation PONs (NG-PONs) that can be implemented in the current infrastructure without the need for a major overhaul, yielding in low capital expenditure (CAPEX) [3], all while offering customers security, protocol- and bitrate-transparency, and large scalability and upgradability, besides retaining a very small number of optical fibers, resulting in a significantly lower operating expenditure (OPEX) of the optical networks [4].

To this end, self-assembled InAs/InP quantum dash (Qdash) nanostructure-based laser diodes emerge as potential light sources with demonstrated emission in a wide range of wavelengths covering the S-, C-, L-, and U-bands [5]–[7]. In particular, mid and far L-band Qdash laser diodes (QDLD) are of great interest from the outlook of future NG-PONs whose primary goal is maximizing the per-user capacity and increasing the number of possible subscribers, in addition to increasing the network range [1], [2]. Hence, L-band QDLD diode-based transmitters would enable extending the operational bandwidth from the well-exhausted C-band to the neighboring L-band, as a natural evolution [3], and standout as prime candidates for realizing this promising approach. Moreover, these quantum confined nanostructure-based lasers possess niche features such as compact size, low power consumption, integrability in hybrid optical-silicon systems [8], [9], and more importantly their inherent broadband gain profiles due to inhomogeneous dash sizes owing to the self-assembly growth process. Although this latter feature seems a disadvantage for lasers, however, has been exploited to realize 1550 nm multiwavelength QDLD or comb sources [7], which has consequently, qualified them as promising contenders for source-unified NG-PON paradigms [10].

Several demonstrations have been reported in the literature on the employment of 1550 nm InAs/InP Qdash multiwavelength mode-locked Fabry-Perot (FP) laser sources in single point-to-point as well as point-to-multipoint WDM optical systems. For instance, a single Qdash mode-locked laser has been employed as multi-wavelength optical source by extracting 8 separate longitudinal modes as channels for 80 Gbits/s-50 km single-mode fiber (SMF) (8 × 10 Gbits/s) transmission utilizing on-off keying (OOK) [11], and later 12 Tbits/s–75 km SMF WDM transmission employing 32 quadrature amplitude modulation (32QAM) on 60 channels [12]. Thanks to the inherent mode-locking characteristics observed from these nanostructure-based multiwavelength lasers that enabled significant improvement in device RF characteristics. Moreover, further improvements to optical linewidths (Δf_L) and phase noise (S_φ) of the channels (*i.e.*, each longitudinal mode) are achieved via additional assisting techniques. These include injection locking [12] and external hardware components [13], in addition to improving the coherent detection performance via sophisticated algorithms such as symbol-wise blind phase search (BPS) [14]. Very recently, an aggregated data rate of 10 (5.376) Tbits/s was reported over a single 1550 nm Qdash mode-locked laser with 38 (48) channels in a 16QAM (four-level pulse amplitude modulation (PAM-4)) modulation scheme [15] ([8]).

Nevertheless, deployment of InAs/InP QDLD for WDM transmission in L-band has not been explored yet, to the authors' knowledge. Nonetheless, the only L-band WDM transmission reports in literature are limited to employing either commercial external cavity lasers (ECLs) or distributive feedback (DFB) lasers. For instance, 360 WDM channels (∼1528-1606 nm) employing 180 lasers with 257 Tbits/s over 48-km long 10-mode fiber utilizing quadrature-phase shift keying (QPSK) was reported in [16]. This was then pushed to 10.16 Peta-bit/s via hybrid WDM-mode and space division multiplexing approaches on 6-mode 19-core fiber [17]. In another report, a 100-channel WDM system with 10 Gbits/s channel data transmission was demonstrated via 54 ECLs and 46 DFB

lasers in the L-band ($\sim$1570–1590 nm) over 400-km long fiber [18]. In [19], 80 DFB lasers were employed to achieve 3.2 Tbit/s (80 $\times$ 42.7 Gbits/s) WDM transmission over 20 $\times$ 100 km fiber covering $\sim$1570–1603 nm.

Hence, in this work, we demonstrate the first L-band ($\sim$1610 nm) WDM transmission to be reported over an InAs/InP QDLD. This was carried out by first injection-locking a single longitudinal mode of the multimode QDLD to enhance its Δf_L and noise characteristics. Afterwards, the injection-locked QDLD (IQDL) is used in tandem with a comb generation technique, which is based on phase modulation, to generate three 50-GHz spaced channels, thus realizing an IQDL comb source (IQDL-CS). This method of comb generation is adopted because the QDLD exhibited inferior RF characteristics, indicating a negligible mode locking characteristics. Later, by deploying this source, we demonstrate an aggregate 192 Gbit/s (3 $\times$ 64 Gbit/s), 3-channel L-band DWDM transmission over a 10-km SMF utilizing a dual-polarization QPSK (DP-QPSK) modulation scheme. In addition, a comprehensive investigation of the Δf_L, $S\varphi$, and frequency noise effects on the transmission performance are evaluated, showing minimum values of 44 kHz, -80 dBc/Hz, and 5.2×10^{11} Hz^2/Hz, respectively. This work constitutes the first step towards the exploration of quantum-confined nanostructure-based lasers in L-band WDM infrastructures in realization of future NG-PONs' outlooks and requirements.

2. Experimental Setup

In this section, various setups employed in the present work are discussed besides summarizing about the InAs/InP QDLD and the subsequent comb source generation.

2.1 L-band InAs/InP QDLD

The investigation in this work is carried over a bare 4 $\times$ 700 μm^2 ridge-waveguide L-band quantum dash-in-a-well laser diode whose device structure and scanning electron microscope (SEM) image of the facet are illustrated in the inset of Fig. 1(a). The self-organized InAs Qdash chirped active region device structure was grown by molecular beam epitaxy (MBE) on a (100) oriented S-doped n-type InP substrate. The QDLD is in a *p-i-n* configuration with a 200-nm thick In$_{0.52}$Ga$_{0.28}$Al$_{0.2}$As undoped separate confinement heterostructure (SCH) layer lattice-matched to the InP substrate. The waveguide core center comprises of the undoped quantum-dash-in-asymmetric-well active region with 4 alternating stacks of 1.3-nm thick compressively strained In$_{0.64}$Ga$_{0.16}$Al$_{0.2}$As quantum well layer, a 5-ML thick InAs dash layer, and a 6.3 nm thick compressively strained In$_{0.64}$Ga$_{0.16}$Al$_{0.2}$As quantum well layer. Each stack is topped by a tensile-strained In$_{0.50}$Ga$_{0.32}$Al$_{0.18}$As top barrier layer on a single In$_{0.50}$Ga$_{0.32}$Al$_{0.18}$As 25-nm thick lower barrier layer. The structure was chirped by varying the thickness of each top barrier layer, *viz.* 10, 10, 15, and 20 nm, in order to increases the inhomogeneity of the structure and achieve a broader gain profile [20]. The as-cleaved bare QDLD was mounted over a brass base and probed via a laser source-meter (Keithley 2520) while its temperature is controlled by a thermoelectric cooler (TEC, Keithley 2510). The right inset of Fig. 1(b) shows the single-facet continuous wave (CW) L-I curve of the QDLD at 14 °C exhibiting a threshold current (I_{th}) of $\sim$100 mA, which corresponds to a threshold current density (J_{th}) of $\sim$3.57 kA/cm^2, and a near-threshold slope efficiency of 0.106 W/A. The reason to operate at lower temperature was two folds; firstly to minimize the junction heating-induced wavelength red shifting as the L-band QDLD is an un-optimized grown device structure unlike the reported high-quality Qdash laser diodes operating in the C-band platform; and secondly, to operate within the wavelength limitations of the L-band compatible optical communication system components and equipment.

2.2 L-band InAs/InP IQDL-CS

The top leftmost dashed box in Fig. 1(a) depicts the block diagram to generate IQDL comb source (IQDL-CS), whose longitudinal modes serve as separate channels for the DWDM transmission.
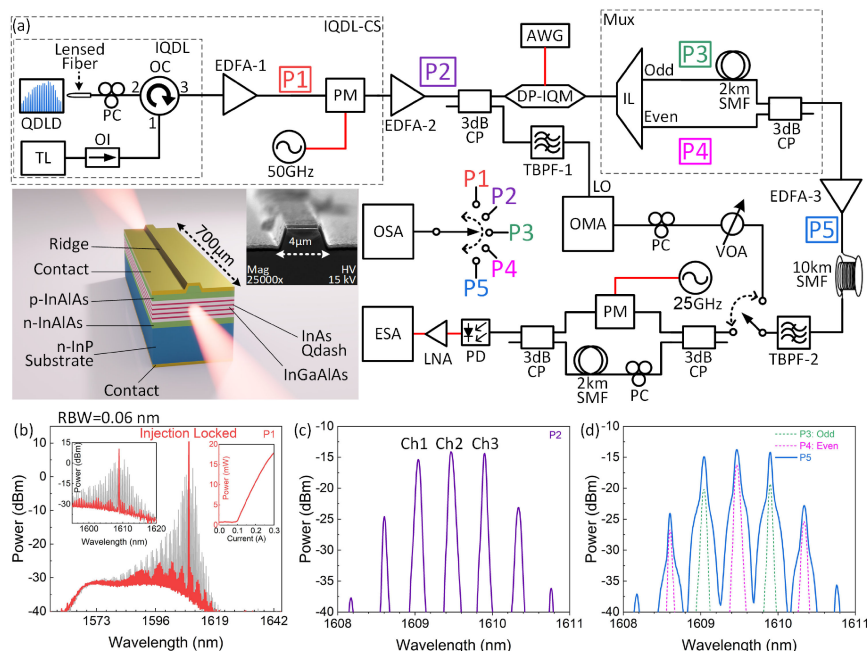
Fig. 1. (a) Experimental system setup utilized for far L-band DWDM transmission and characterization over the IQDL-CS where black lines denote optical connections while red ones represent electrical connections. The inset of (a) shows the epitaxial structure and an SEM image of the QDLD. The lasing emission spectra shown at different locations in the system, for (b) IQDL and QDLD (P1), (c) the generated comb lines from the IQDL-CS (P2), and (d) the unmodulated demultiplexed odd and even modes of IQDL-CS (P3 and P4) alongside the combined 32 Gbaud modulated optical spectrum (P5). The right inset of (b) depicts the CW single facet L-I characteristics of the QDLD at 14 °C, while its left inset shows a zoomed-in portion of the optical spectrum. TL: tunable laser; PC: polarization controller; OI: optical isolator; OC: optical circulator; EDFA: Erbium doped fiber amplifier; CP: optical coupler; PM: phase modulator; SMF: single mode fiber; TBPF: tunable bandpass filter; DP-IQM: dual-polarization I/Q modulator; IL: optical interleaver; LO: local oscillator; VOA: variable optical attenuator; OMA: optical modulator analyzer; PD: photodetector; LNA: low-noise amplifier; ESA: electrical signal analyzer; OSA: optical spectrum analyzer; RBW: resolution bandwidth; AWG: arbitrary wave generator.

At an operating current of $1.1I_{th} = \sim 110$ mA, the QDLD's single facet power is butt-coupled manually using a three-axis translation stage into a lensed SMF passing the lasing emission into port 2 of an optical circulator (OC). The coupled fiber optical power was measured to be 0.5 mW corresponding to a coupling efficiency (loss) of $\sim 5\%$ (~ -13 dB). A tunable laser (TL, Agilent 81600B) was then utilized as a master laser and tuned to a single mode at 1609.47 nm to first injection-lock the multimodal emission of the QDLD into a single Fabry–Pérot (FP) mode [21], [22] at 1609.47 nm (~ 0 detuning) through port 1 of the OC, at an injection ratio (IR, ratio between injected TL power to the slave QDLD power) of -10 dB. According to our preliminary investigation, IR plays a role in affecting the characteristics of injection locking; Particularly, higher IR resulted in narrower optical linewidths and lower phase noise. Hence, an IR of -10 dB was adopted to perform the DWDM transmission experiment in the present work as it was the maximum IR possible with our equipment. Nevertheless, the IQDL's emission is then passed through port 3 of the OC to be amplified by an L-band Erbium-doped fiber amplifier (EDFA-1, Amonics AEDFA-L-18BR). Fig. 1(b) compares the lasing spectra of both the QDLD and single mode IQDL that is obtained at location P1 via an optical spectrum analyzer (OSA, Agilent 86142b) with a resolution bandwidth (RBW) of 0.06 nm. The multimode QDLD spectrum is centered at ~ 1610 nm with a 3 dB bandwidth of ~ 7 nm while the IQDL mode exhibited > 35 dB side mode suppression ratio (SMSR). Note that the amplified spontaneous emission (ASE) hump of EDFA-1, visible in Fig. 1(b), shows operation at its amplification window edge, thus limiting the gain associated with the 1609.47 nm IQDL mode.

This mode is then passed into a phase modulator (PM) driven by a 50-GHz signal to realize the IQDL-CS. In this configuration, the PM creates the side harmonics at either side of the locked mode with an exact spacing equal to the driving frequency, *i.e.,* 50 GHz, matching the international telecommunication union (ITU) DWDM transmission grid. The number of generated harmonics and their amplitudes are controlled by adjusting the amplitude of the 50-GHz RF drive signal. In this work, six side harmonics were generated while the power of the first two side harmonics are aligned with the main mode to be used in conjunction, thus exhibiting a comb source with 7 carriers. The central three modes, located at 1609.04, 1609.47, and 1609.90 nm, are then employed as sub-carriers in 3-channel DWDM transmission. The IQDL-CS is later amplified by EDFA-2, and the resulting multi-wavelength spectrum at location P2 is shown in Fig. 1(c) indicating the seven comb lines, with the three central lines Ch1, Ch2, and Ch3, exhibiting peak optical power flatness of <1.0 dB and optical signal to noise ratio (OSNR) of ∼30 dB.

2.3 DWDM Transmission Setup

The amplified output of the IQDL-CS at location P2 is split via a 3 dB coupler where one branch is used for modulation and transmission purpose while the other serves as a local oscillator (LO) signal during coherent detection at the receiver. All the sub-carriers were then modulated by a LiNbO$_3$ Mach-Zehnder based dual-polarization in-phase/quadrature modulator (DP-IQM) using a pre-processed data signal via MATLAB by generating a pseudo random binary sequence (PRBS) with a length of $2^{11}-1$ via an arbitrary wave generator (AWG, Keysight M8195A) and an applied RRC filter with a roll-off factor of 0.35 for Nyquist pulse shaping, which is mapped into a two-level electrical signal in order to obtain the QPSK format. Thereafter, the modulated signals were demultiplexed into even and odd components via an L-band interleaver (IL), uncorrelated via a 2-km long SMF, again combined (multiplexed) via another 3 dB coupler, pre-amplified by EDFA-3, and then transmitted over a 10-km long SMF. Fig. 1(d) depicts the emission spectrum of the 32-Gbaud modulated IQDL-CS (location P5) alongside the superimposed spectra (dashed-lines) of the respective unmodulated odd and even modes, measured at locations P3 and P4, respectively. A clear separation of the even and odd modes is apparent from Fig. 1(d) showing no sign of crosstalk. Moreover, a broadened −3 dB optical linewidth in all channels is evident from the figure, a signature of modulated carriers. The maximum transmitted baud rate in this work is 32 Gbaud utilizing a QPSK modulation scheme with a 0.35-roll off factor (*i.e.,* 43.2 GHz); therefore, exhibiting at least 6.8 GHz guard band between the adjacent channels and minimizing the crosstalk interference effects. Hence, an optical spectral efficiency of 1.2−1.8 and 2.4−3.6 bits/s/Hz are estimated for the QPSK and DP-QPSK modulation schemes, respectively.

At the receiver side, a tunable bandpass filter (TBPF-2, Santec-350 with a tunable bandwidth of 0.1−15 nm) is used as a demultiplexer to receive the designated channel for demodulation selectively. Both TBPF-1 and TBPF-2 were simultaneously and identically tuned, where the former was utilized to pass the matching LO signal while the latter passes the desired channel signal. Both signals were then received by an optical modulation analyzer (OMA, Keysight N4391A) which performed coherent detection and post signal processing, including, timing recovery, phase recovery, root-raised-cosine filtration, frequency offset compensation, BPS, and adaptive equalization, to recover the modulating signal. Lastly, a variable optical attenuator (VOA, Keysight VOA-N7764A) was also used to control the power of the received signal for investigation purposes. It is noteworthy to point out here the challenging endeavor of conducting optical communication investigation in the mid-to-far L-band window due to the limited/unavailability of wavelength-compatible optical communication equipment and components. This is ascribed to the underexplored nature of the mid-to-far L-band as a platform for optical communications.

2.4 RF Characterization Setup

A modified self-heterodyne technique was employed in order to measure the RF characteristics of the designated channel either before modulation (at location P2 after passing through a TBPF)

or after transmission (*i.e.,* before demodulation of the received signal) by down-converting its frequency. A 25 GHz-driven phase modulator was used to generate its side harmonics at a frequency separation of 25 GHz. The signal was then beaten with its side harmonics via a 3 dB coupler and a 70-GHz photodetector (XPDV3120). This differs from the traditional self-heterodyne technique, where the signal under investigation is beaten with a frequency-shifted version of itself [23]. Nonetheless, the beat tone was then amplified via a low-noise amplifier (LNA) and passed to an electrical signal analyzer (ESA, Keysight N9010B) to measure the linewidth and $S\varphi$ characteristics. Since the bandwidth of the ESA is 44 GHz, only the beat tone between the signal and its first harmonic (25 GHz) was detected and analyzed.

3. Results and Discussion

In general, the highly dispersive size of self-assembled Qdashes are intrinsically associated with multimode QDLD emission exhibiting relatively inferior RF characteristics such as broad Δf_L (tens and hundreds of MHz) and high noise floors. Consequently, this renders employment of these modes as individual subcarriers in optical communications obsolete. Therefore, in literature, assisting method such as mode-locking have been exclusively employed to improve the RF characteristics of 1550 nm QDLD to enable demonstration of a single frequency comb source with tens of modes as individual sub-carriers, thanks to the well optimized growth as well as the laser device structure design in the 1550- region. However, mode-locking from a single-section L-band QDLD has not been observed in the present work, which is possibly due to the unoptimized growth and laser device structure design. Hence, injection-locking assisting scheme in tandem with the PM based comb generation technique is employed to realize an IQDL-CS for DWDM system demonstration. In principle, this source could be replaced by a mere single L-band QD MLL should mode-locking be demonstrated in near future.

3.1 RF Characteristics of IQDL-CS

The RF characteristics of the unmodulated three channels, Ch1, Ch2, and Ch3, of the IQDL-CS were obtained in terms of Δf_L (calculated via Lorentzian fitting with an error margin of ± 1 kHz), $S\varphi$, and frequency noises. The electrical spectra of the respective down-converted three sub-carriers are shown in Figs. 2(a)–(c) alongside the corresponding Lorentzian fitted curves. At first glance, it can be observed that IQDL-CS central channel (Ch2), exhibits the broadest Lorentzian linewidth Δf_L of 50 kHz whereas Ch1 and Ch3 displayed Δf_L of 44 and 45 kHz, respectively. This can be attributed to the interference exhibited in the central channel due to the two adjacent ones, while each of the side channels, *i.e.,* Ch1 or Ch3, only exhibits interference from a single channel, Ch2. Thereafter, the low-frequency $S\varphi$ is obtained for Ch1, Ch2, and Ch3 and are shown in Figs. 2(d)–(f), respectively. Besides, the corresponding frequency noise spectral densities (S_v) are also shown in the respective insets of Figs. 2(d)–(f), which are calculated according to [24]:

$$S_v\ (f) = \ S\varphi\ (f)\ .\ f^2 \tag{1}$$

where f is the frequency. It is to be noted that the OMA at the receiver end implements symbol-wise phase tracking algorithm (*i.e.,* blind phase search); thus, the only phase-noise-related factors affecting the QPSK transmission are the linewidth and low-frequency noise, as discussed in [15]. Furthermore, since the Δf is fundamentally determined by the low-frequency part of the noise spectrum [25], the present noise investigation of the channels has been confined to low frequencies of up to 6 MHz and a comparative analysis is performed at $f = 1$ kHz. Considering Figs. 2(d)–(f), the IQDL-CS exhibited $S\varphi$ values of -80, -76, and -79 dBc/Hz for Ch1, Ch2, and Ch3, respectively. These inferior characteristics of the central channel compared to the adjacent channels of both comb sources, are in good agreement with the observed linewidth trend of Figs. 2(a)–(c) thus substantiating our discussion of dependence of linewidth on the low-frequency noise. Furthermore, since S_v is proportional to $S\varphi$ with a factor of f^2, the former noise again depicted a similar trend of inferior performance of Ch2 compared to Ch1 and Ch3. In this case, the calculated values of S_v are
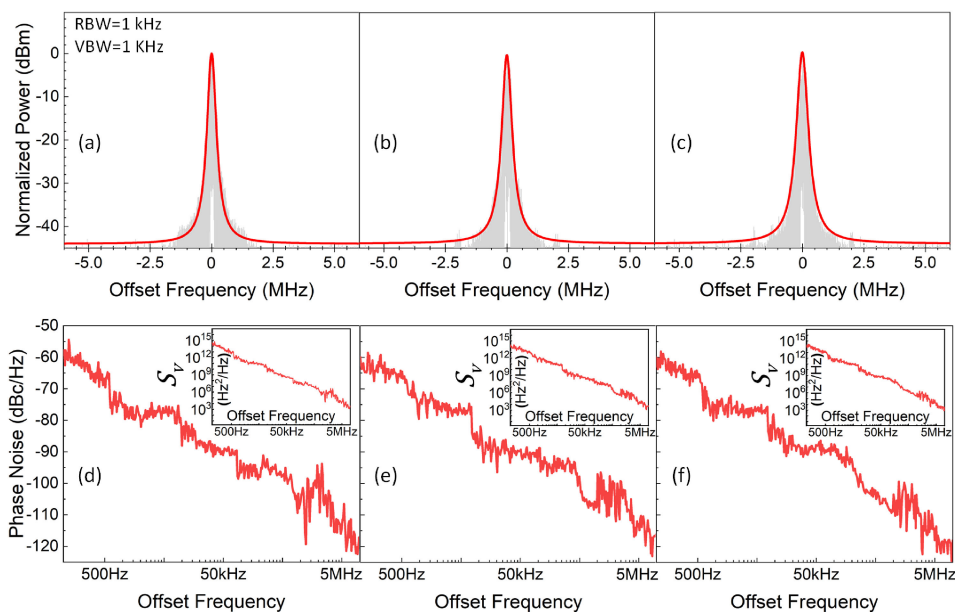
Fig. 2. Measured RF spectrum of (a) Ch1, (b) Ch2, and (c) Ch3 of the IQDL-CS alongside the Lorentzian fitted curves. In addition, the measured S_φ curves is shown for (d) Ch1, (e) Ch2, and (f) Ch3, respectively, with corresponding insets depicting the calculated frequency noise spectral densities for the respective channel.

5.2×10^{11}, 6.9×10^{11}, and 5.4×10^{11} Hz^2/Hz for Ch1, Ch2, and Ch3, respectively. Furthermore, the same performance trend was observed at offset frequencies of 10 and 100 kHz as well.

3.2 Coherent DWDM Transmission

For the transmission experiment, the DP-QPSK scheme was employed to externally modulate the three channels via the DP-IQM modulator shown in Fig. 1(a), with different symbol rates of 16(32), 28(56), and 32(64) Gbaud (Gbit/s) and transmitted through 10 km SMF to characterize the transmission performance of the IQDL-CS. Figs. 3(a)–(c) show the measured BER (evaluated based on the error vector magnitude (EVM) of the recovered and decoded signals on the OMA) at different symbol rates, as functions of the received optical power, obtained separately for Ch1, Ch2, and Ch3. Besides, transmission measurements for the back-to-back (BtB) configuration at 32 Gbaud are also plotted in Figs. 3(a)–(c) for comparison purpose. The insets of Figs. 3(a)–(c) depict the respective channel's received QPSK constellation and eye diagrams for a single polarization at 28 and 32 Gbaud. In coding theory, Forward-Error Correction (FEC) is an error correction technique that can detect and correct errors that occur in the transmission path and is incorporated by several vendors in 10G and 40G optical networks [26]. For example, Hard-Decision FEC can achieve corrected BERs as low as 10^{-15} using a 7%-overhead with a net coding gain (NCG) of 9.19 dB, which for all intents and purposes is considered error-free [27]. According to the ITU-T G.975.1 recommendations, the pre-FEC BER should be less than 3.8×10^{-3} [28]. As such, an error-free 32 Gbaud (64 Gbit/s) transmission was achieved for all the three channels with a BER below the 7%-overhead Forward-Error Correction (FEC) threshold of 3.8×10^{-3} at a received power of $\sim{-}11$ dBm. This translates to an aggregate data rate of 192 Gbit/s (3 channels $\times$ 64 Gbit/s per channel) of the DWDM system. To the best of the authors' knowledge, this constitutes the highest data rate to be reported in the far L-band and the first demonstration of a DWDM system around the $\sim$1610 nm window using a quantum-confined semiconductor laser source. Furthermore, although a DP-QPSK modulation scheme was adopted in the transmission, due to equipment limitations, only one of the two received polarizations was analyzed. In other words, by including the second
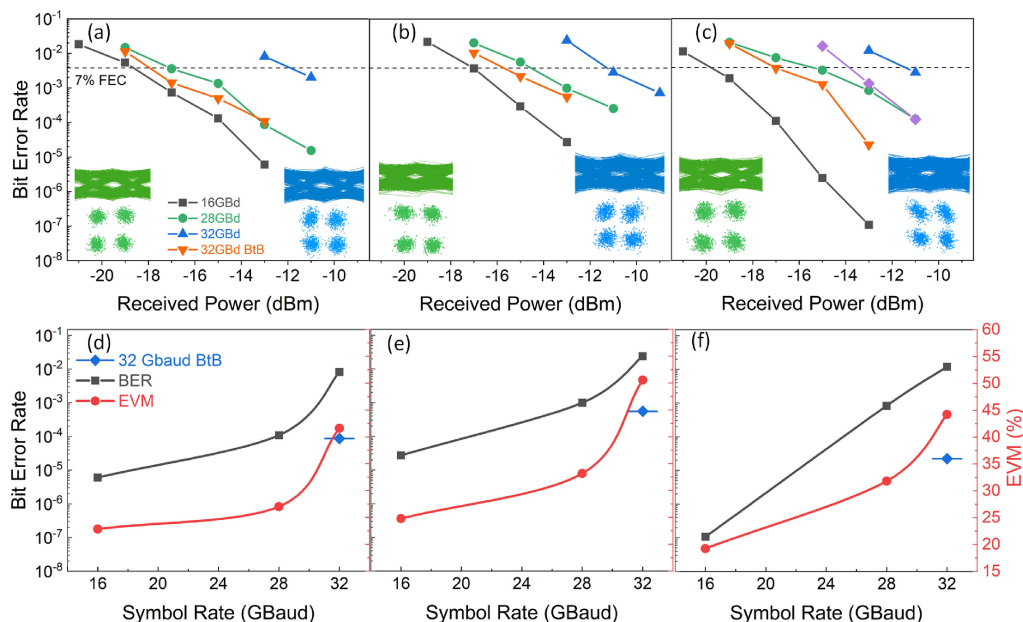
Fig. 3. DWDM transmission BER as a function of the received power for (a) Ch1, (b) Ch2, and (c) Ch3 at different symbol rates, over a 10-km long SMF, and alongside the BtB case at a symbol rate of 32 Gbaud as a reference case for each respective channel. The insets of (a)–(c) show the corresponding constellation and eye diagrams of 28 and 32 Gbaud symbol rates for each respective channel. In addition, the extracted BER and EVM values are summarized for (d) Ch1, (e) Ch2, and (f) Ch3 alongside the BtB reference case.

received polarization, which should show a similar performance to the other one as we have observed in our previous works [6], [10], the effective aggregate data rate would double, *i.e.,* 384 Gbit/s. It is to be noted that the number of unified optical power channels and their wavelength selection are constrained by the comb generating circuit and the limited bandwidths of various equipment (EDFA, TBPF, and OMA), respectively. In principle, the IQDL's lasing emission covers beyond 1625 nm; however, these limitations restricted the wavelength of operation to ∼1610 nm and DWDM transmission demonstration to over simultaneous 3 channels.

Next, the power penalty exhibited by various channels is investigated. Fig. 3(b) shows that a minimum received power of −15.8 dBm is required by Ch2 to attain a BER below the FEC limit in the BtB case. This value increases to −11.4 dBm through the 10-km SMF, yielding in a difference of 4.4 dB. Nonetheless, given that the SMF exerts an attenuation rate of 0.2 dB/km (2dB total attenuation), this translates to a leeway of 2.2 dB between the 10-km SMF and BtB transmission after excluding the fiber attenuation effect. The left (right) channel, on the other hand, as depicted in Fig. 3(a) (Fig. 3(c)), displayed a corresponding wider leeway of 4.0 (3.5) dB since it exhibited lower minimum required received power of −18(−17.1) dBm for successful 32-Gbaud BtB transmission. In other words, Ch2 was observed to be more restricted in terms of minimum received power for error-free transmission than either side channels and hence expected to show mediocre transmission performance at a unified received power for all channels. This again is in good agreement with our earlier discussion about the inferior RF characteristics of Ch2 followed by Ch3 and then Ch1. In fact, the aforementioned minimum required received powers among the different channels complies with a similar trend that was observed between them in terms of their RF characteristics. Moreover, the DWDM demonstration has resulted in an OSNR penalty of ∼1.5–2.5 dB observed at the highest modulation symbol rate of 32 Gbaud.

To further investigate the performance of the system, Figs. 3(d)–(f) summarize the measured BER and EVM at a received power of −13 dBm for Ch1, Ch2, and Ch3, respectively, at different symbol rates, besides the 32 Gbaud BtB reference case. As pointed out earlier, the central channel
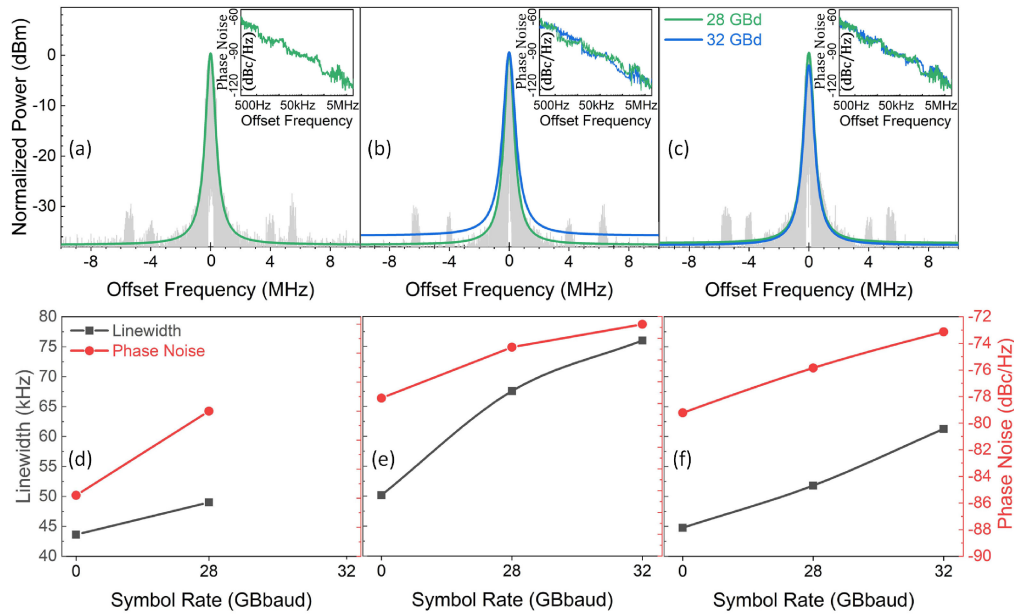
Fig. 4. Measured RF spectrum of (a) Ch1, (b) Ch2, and (c) Ch3 at RBW and VBW of 1 kHz, modulated at 28 Gbaud, alongside the Lorentzian fitted curves for the 28 and 32 Gbaud symbol rates. The insets show the measured phase noise for Ch1, Ch2, and Ch3, respectively. A summary of the measured Δf_L and S_φ for (d) Ch1, (e) Ch2, and (f) Ch3 for symbol rates of 0 (unmodulated case), 28, and 32 Gbaud.

(Ch2) displayed an inferior performance with higher BER's (EVM's) when compared to either side channels for all data rates. For instance, at 32 Gbaud, Ch2 displayed a BER (EVM) value of 2.4×10^{-2} (50.6%) whereas Ch1 and Ch3 channels showed 8×10^{-3} (41.6%) and 1.2×10^{-2} (44.2%), respectively, at a fixed -13 dBm received power (below the minimum required power for successful transmission). In short, at high data rates, the channel linewidth and low-frequency noise play a significant role in determining the transmission performance. In other words, broader channel optical linewidths result in a greater degree of pulse broadening, chromatic dispersion, and crosstalk between the adjacent channels, and thus limits the DWDM system performance.

In order to shed further insight into the effect of modulation on the features of the carrier signals and hence the DWDM system performance, in the following, we investigate the RF characteristics of the modulated channels at the receiver end before demodulation. The measured electrical spectra and S_φ curves are plotted in Figs. 4(a)–(c) for Ch1, Ch2, and Ch3, respectively, alongside the respective Lorentzian fitted linewidths, for 28 and 32 Gbaud. Nevertheless, at first glance, it can be observed that the higher 32 Gbaud symbol rate significantly increased S_φ (see respective insets) and subsequently, the Δf_L, which is most notably for the central channel (Ch2). This has been systematically summarized in Figs. 4(d)–(f) that plot Δf_L and S_φ of Ch1, Ch2, and Ch3, respectively, for symbol rates of 0 (unmodulated case), 28, and 32 Gbaud. An apparent increase in S_φ of Ch2 from -76 (unmodulated) to -70 dBc/Hz (28 Gbaud), translating to a ~6 dBc/Hz increase is recorded. On the other hand, the corresponding rise in S_φ by ~5 (~3) dBc/Hz is observed from Ch1 (Ch3). Accordingly, Ch2 experienced the largest increase in Δf_L from ~53 to ~68 (~28% increase) to ~76 kHz for the unmodulated, 28, and 32 Gbaud modulated signals. On the other hand, the corresponding values of ~48 to ~52 (~8% increase) to ~61 kHz and ~46 to ~48 kHz (~4% increase) are exhibited by Ch3 and Ch1, respectively. Also, the broadened Δf_L at higher data rates is also reflected in the 32 Gbaud modulated optical emission spectrum, depicted in Fig. 1(d), where an increase in the -3 dB bandwidth of Ch1, Ch2, and Ch3 from 56.4, 60.3, and 45.2 pm (unmodulated) to 64.3, 71.4, and 53.2 pm (modulated), corresponding to an increase of 14, 18.4, and 17.7% is noted. Hence, these measurement results from various aspects yet again

substantiate the inferior transmission performance of the central channel compared to the other channels and in part, elucidates the increased power penalty of Ch2 at higher dates to reach the FEC limit since more signal power is required to compensate for the noise to attain error-free transmission.

4. Conclusion

An injection-locked InAs/InP quantum dash bare laser diode-based 3-channel comb source in the mid L-band wavelength window is demonstrated. An error-free DWDM transmission around ~1610 nm window is demonstrated over three simultaneous 50-GHz spaced channels from this single IQDL-CS, with an aggregate data rate of 192 (3 × 64) Gbit/s over a 10-km SMF channel. The RF characteristics in terms of Δf_L, $S\varphi$, and S_v are then investigated for all three channels. The investigation showed that the central channel exhibited significantly broader Δf_L and worse low-frequency noise characteristics compared to the side channels. These observations reflected on the performance of the transmission over each respective where broader linewidths (and higher noise at low-frequency offsets) correlated to higher power penalties and higher BER at fixed received powers, due to postulated increased crosstalk, chromatic dispersion, and pulse spreading. The results open the door to widening the operation window of WDM systems to the under-utilized L-band in order to meet the requirements of NG-PON of unified sources and broader bandwidths. With further optimization and availability of compatible equipment, the performance of the WDM would improve significantly.

References

[1] Cisco. "Cisco visual networking index: Global mobile data traffic forecast update, 2016–2021. White Paper," ed, 2019.
[2] Cisco. "Cisco Annual Internet Report (2018–2023) White Paper," ed, 2020.
[3] D. Nesset, "PON roadmap [invited]," *IEEE/OSA J. Opt. Commun. Netw.*, vol. 9, no. 1, pp. A71–A76, Jan. 2017.
[4] E. Wong, "Next-Generation broadband access networks and technologies," *J. Lightw. Technol.*, vol. 30, no. 4, pp. 597–608, Dec. 2011.
[5] M. Z. M. Khan, T. K. Ng, and B. S. Ooi, "Self-assembled InAs/InP quantum dots and quantum dashes: Material structures and devices," *Progress Quantum Electron.*, vol. 38, no. 6, pp. 237–313, Nov. 2014.
[6] M. A. Shemis *et al.*, "Broadly tunable self-injection locked InAs/InP quantum-dash laser based fiber/FSO/hybrid fiber-FSO communication at 1610 nm," *IEEE Photon. J.*, vol. 10, no. 2, Feb. 2017, Art. no. 7902210.
[7] E. Alkhazraji, M. S. Alias, K. K. Qureshi, and M. Z. M. Khan, "Monolithic tunable InAs/InP broadband quantum-dash laser," *IEEE Access*, vol. 8, pp. 39046–39055, Feb. 2020.
[8] G. Liu *et al.*, "Passively mode-locked quantum dash laser with an aggregate 5.376 Tbit/s PAM-4 transmission capacity," *Opt. Express*, vol. 28, no. 4, pp. 4587–4593, Feb. 2020.
[9] Z. Lu, *Quantum-Dot Coherent Comb Lasers for Terabit Optical Networking Systems (SPIE OPTO)*. San Francisco, USA: SPIE, 2019.
[10] M. A. Shemis *et al.*, "L-Band quantum-dash self-injection locked multiwavelength laser source for future WDM access networks," *IEEE Photon. J.*, vol. 9, no. 5, Jul. 2017, Art. no. 7905807.
[11] A. Akrout *et al.*, "Separate error-free transmission of eight channels at 10 gb/s using comb generation in a quantum-dash-based mode-locked laser," *IEEE Photon. Technol. Lett.*, vol. 21, no. 23, pp. 1746–1748, Sep. 2009.
[12] J. N. Kemal *et al.*, "32QAM WDM transmission using a quantum-dash passively mode-locked laser with resonant feedback," in *Proc. Opt. Fiber Commun. Conf. Exhib.*, pp. 1–3, Jun. 2017.
[13] J. Pfeifle *et al.*, "Simultaneous phase noise reduction of 30 comb lines from a quantum-dash mode-locked laser diode enabling coherent tbit/s data transmission," in *Proc. Opt. Fiber Commun. Conf. Exhib.*, Jun. 2015, pp. 1–3.
[14] T. Pfau, S. Hoffmann, and R. Noe, "Hardware-efficient coherent digital receiver concept with feedforward carrier recovery for M-QAM constellations," *J. Lightw. Technol.*, vol. 27, no. 8, pp. 989–999, Apr. 2009.
[15] P. Marin-Palomo *et al.*, "Comb-based WDM transmission at 10 Tbit/s using a DC-driven quantum-dash mode-locked laser diode," *Opt. Express*, vol. 27, no. 22, pp. 31110–31129, Oct. 2019.
[16] D. Soma *et al.*, "257-Tbit/s weakly coupled 10-Mode C + L-Band WDM transmission," *J. Lightw. Technol.*, vol. 36, no. 6, pp. 1375–1381, Jan. 2018.
[17] D. Soma *et al.*, "10.16-Peta-B/s dense SDM/WDM transmission over 6-Mode 19-core fiber across the C+L band," *J. Lightw. Technol.*, vol. 36, no. 6, pp. 1362–1368, Mar. 2018.
[18] A. K. Srivastava *et al.*, "Ultradense WDM transmission in L-band," *IEEE Photon. Technol. Lett.*, vol. 12, no. 11, pp. 1570–1572, Nov. 2000.
[19] B. Zhu *et al.*, "3.2 Tb/s (80 × 42.7Gb/s) transmission over 20 × 100km of non-zero dispersion fiber with simultaneous C + L-band dispersion compensation," in *Proc. Opt. Fiber Commun. Conf.*, Mar. 2002, Paper. FC8, vol. 70, Anaheim, California.

[20] J. X. Chen *et al.*, "Tuning InAs/GaAs quantum dot properties under Stranski-Krastanov growth mode for 1.3 μm applications," *ACS Photon.*, vol. 91, no. 10, pp. 6710–6716, 2002.

[21] R. Lang, "Injection locking properties of a semiconductor laser," *IEEE J. Quantum Electron.*, vol. QE-18, no. 6, pp. 976–983, Jun. 1982.

[22] C. Yeh *et al.*, "Performance of long-reach passive access networks using injection-locked Fabry–Perot laser diodes with finite front-facet reflectivities," *J. Lightw. Technol.*, vol. 31, no. 12, pp. 1929–1934, Jun. 2013.

[23] T. Okoshi, K. Kikuchi, and A. Nakayama, "Novel method for high resolution measurement of laser output spectrum," *Electron. Lett.*, vol. 16, no. 16, pp. 630–631, Jul. 1980.

[24] M. Schiemangk, S. Spießberger, A. Wicht, G. Erbert, G. Tränkle, and A. Peters, "Accurate frequency noise measurement of free-running lasers," *Appl. Opt.*, vol. 53, no. 30, pp. 7138–7143, Oct. 2014.

[25] L. N. Binh, *Optical Modulation: Advanced Techniques and Applications in Transmission Systems and Networks*. Boca Raton, FL, USA: CRC Press, 2017.

[26] M. Scholten, T. Coe, J. Dillard, and F. Chang, "Enhanced FEC for 40G/100G," in *Proc. ECOC*, 2009, WS1, pp. 1–12.

[27] J. Cho, C. Xie, and P. J. Winzer, "Analysis of soft-decision FEC on non-AWGN channels," *Opt. Express*, vol. 20, no. 7, pp. 7915–7928, 2012.

[28] I. T. UNION, "ITU-T G.975.1," in *Appendix I*. Feb. 2004.